ORIGINAL ARTICLE

Effect of dental malocclusion on cerebellar neuron activation via the dorsomedial part of the principal sensory trigeminal nucleus

Minghong Shi[1,2] | **Xin Liu**[2,3] | **Chunkui Zhang**[4] | **Hongyun Zhang**[2] | **Qian Liu**[2] | **Dongmei Wang**[1] | **Xiaodong Liu**[2] | **Jinlian Li**[4] | **Meiqing Wang**[1,2]

[1]School of Stomatology, The Third Affiliated Hospital of Xinxiang Medical University, Xinxiang, China

[2]Department of Oral Anatomy and Physiology, School of Stomatology, The Fourth Military Medical University, Xi'an, China

[3]Department of Stomatology, The 960th Hospital of People's Liberation Army, Jinan, China

[4]Department of Anatomy, Histology and Embryology and K.K. Leung Brain Research Centre, The Fourth Military Medical University, Xi'an, China

Correspondence
Meiqing Wang, Department of Oral Anatomy and Physiology, School of Stomatology, The Fourth Military Medical University, Xi'an 710032, China.
Email: mqwang@fmmu.edu.cn

Funding information
National Natural Science Foundation of China, Grant/Award Number: 81870866 and 81920108013; Natural Science Foundation of Shaanxi Province, Grant/Award Number: 2018JM7147

Abstract

Occlusion has been proposed to play a role for body posture and balance, both of which are mediated mainly by the cerebellum. The dorsomedial part of the principal sensory trigeminal nucleus (Vpdm) has direct projection to the cerebellum. The experimental unilateral anterior crossbite (UAC) has an impact on the motor nuclei in the brain stem via trigeminal mesencephalic nucleus (Vme). The current aim was to explore whether UAC has an impact on Vpdm-cerebellum circuit. The inferior alveolar nerve was injected into cholera toxin B subunit (CTb), the cerebellum was injected into fluoro-gold (FG), and the Vpdm was injected into biotinylated dextran amine (BDA) to identify the activation of Vpdm-cerebellum circuit by UAC. Data indicated that there were more neuronal nuclei (NeuN)/CTb/FG triple-labelled neurons and NeuN/CTb/vesicular glutamate transporter 1(VGLUT1) triple-labelled neurons in the Vpdm, and more NeuN/BDA/ VGLUT1 triple-labelled neurons in the cerebellum of rats with UAC than in control rats. The VGLUT1 expression in the Vpdm and cerebellum in the UAC group was higher than that in control rats. These findings indicate an excitatory impact of UAC on the Vpdm-cerebellum pathway and support the role of occlusion for body posture and balance.

KEYWORDS
occlusion, trigeminal mesencephalic nucleus

INTRODUCTION

Dental occlusion is one of the main neurophysiological and pathological stimulators that leads to the activation of periodontal proprioceptive receptors, which are the peripheral processes of the neurons in the trigeminal mesencephalic nucleus (Vme) [1] and trigeminal ganglion [2]. Although still a controversial topic [3–5], studies have indicated that dental occlusion affects the dynamic stability, and the biomechanical and the viscoelastic properties of several muscles, including the sternocleidomastoid, erector spinalis, and the longissimus and masseter muscles [6]. Occlusion has also been reported to have an impact on cervical posture, gait, and motor ability. Several malocclusion traits have been

Minghong Shi and Xin Liu contributed equally to this work.

observed to cause changes in muscle pattern and disorders at the cranial and cervical level, as well as impairments of body balance [6–9]. Hence, dental occlusion disturbance devices negatively impacted the athletic performance of young elite rowers [10] and healthy female subjects [7]. Resistance training with an interocclusal splint improved the lower extremity muscle strength and the balance ability of elderly community dwellers [11]. Since the cerebellum plays a major role in the control and coordination of movement [12], it is interesting to explore the impact of dental occlusion on the cerebellum.

Neurons in the dorsomedial part of the principal sensory trigeminal nucleus (Vpdm) have been proposed to serve different functions, including relaying and processing sensory signals from the head, such as tactility and trigeminal proprioception [13]. The central process of the Vpdm projects to the cerebellum [14]. In the granular layer of crus 1, crus 2, and lobule 9 in the cerebellar cortex, there are projections from the dorsal half of the principal sensory trigeminal nucleus [14–16].

Glutamate is one of the most common excitatory neurotransmitters in the nervous system. Vesicular glutamate transporters play a significant role in signal output for extracellular release by aggregating glutamate into vesicular constituents [17]. The number of vesicular glutamate transporter molecules per synaptic vesicle is thought to have a major impact on the quantal size of glutamatergic neurons, and the variation in vesicular glutamate transporter expression has been suggested to have a significant impact on synaptic transmission [18]. Three isoforms of vesicular glutamate transporters have been identified in the central nervous system [19]. Vesicular glutamate transporter 1 (VGLUT1) and vesicular glutamate transporter 2 (VGLUT2) are considered the most reliable markers for glutamatergic neurons [20]. VGLUT1 mRNA, but not VGLUT2 mRNA, is expressed in the Vme, while VGLUT1 and/or VGLUT2 mRNA are expressed in the Vpdm [21]. The Vpdm contains a high density of differently sized, immunohistochemically heterogeneous neurons, many of which are likely to contain glutamate [22], constituting most of the Vpdm projection neurons [23]. VGLUT-expressing neurons that project from the Vpdm to the contralateral ventral posteromedial thalamic nucleus express VGLUT1 and/or VGLUT2 [24], while most fibres projecting from the Vpdm to the cerebellum only express VGLUT1 [14]. Thus, when neurons in the Vpdm are activated, the VGLUT1 protein expression level in the cerebellum is expected to be increased.

Our recent reports have indicated that neurons in the trigeminal mesencephalic nucleus (Vme) of rats are activated by an experimental unilateral anterior crossbite (UAC) prosthesis [25], which sends excitatory impulses to the trigeminal motor nucleus and then leads to masseter injury [26], atrophy [27], or osteoarthritic lesions in temporomandibular joints [28–32]. Reports have indicated that there are projections from Vme to the trigeminal motor nucleus, facial nerve nucleus, hypoglossal nerve nucleus, nucleus ambiguous, accessory nerve nucleus, and Vpdm [21,33,34]. In UAC treated female rats, the VGLUT1 mRNA expression level of Vme was upregulated [25] and the VGLUT1 protein expression level of trigeminal motor nucleus, facial nerve nucleus, hypoglossal nerve nucleus, nucleus ambiguous, and accessory nerve nucleus was increased [35]. It is of dental interest to determine whether the Vpdm-cerebellum circuit of UAC rats is excited.

In this study, we tested the activation of Vpdm-cerebellum circuit by injecting cholera toxin B subunit (CTb) into the inferior alveolar nerve, fluoro-gold (FG) into the cerebellum, and biotinylated dextran amine (BDA) into Vpdm of UAC treated rats and untreated control rats. We also compared the VGLUT1 expression levels in the Vpdm and cerebellum between the UAC treated and age-matched control rats. The purpose was to detect whether UAC has an excitatory impact on the Vpdm-cerebellum circuit and, thus, to provide supportive evidence for the role of occlusion in body posture and balance.

MATERIAL AND METHODS

Animals

This animal study is one of a series of studies on the UAC model [26–32] and was approved by the Laboratory Animal Care and Welfare Committee, School of Stomatology, Fourth Military Medical University, for animal research (2015-033). All experimental procedures complied with ARRIVE guidelines. Ninety-six female Sprague-Dawley rats (weight 160–180 g) were provided by the Animal Centre of the Fourth Military Medical University. These rats were kept at a temperature of 22–24°C and a normal 12 h–12 h diurnal biological rhythm. All animals could eat and drink freely and adequately during the experiment. Our published data indicated that the mandibular condylar cartilage degeneration in UAC rats was observed as early as 2 weeks. Autophagy in chondrocytes was obvious at 2, 4, and 8 weeks, while apoptosis was enhanced from 8 weeks [28]. In the present study, we collected samples from the animals at 2, 4, and 8 weeks after UAC installation.

Of the 96 rats, 72 were randomly allocated to a UAC group and a control group to be sacrificed at 2, 4, or 8 weeks, respectively ($n = 12$). For each main group and each time point, six rats were used for in situ hybridization immunofluorescence histochemistry, and six rats were used for real-time polymerase chain reaction (PCR) and Western blot analysis (Table 1). The remaining twenty-four rats were randomly divided into a UAC group and a control group. Six rats in each of the UAC and control groups received injections of

TABLE 1 Distribution of the experimental rats in the subgroups

	2 weeks		4 weeks		8 weeks	
	UAC	Con	UAC	Con	UAC	Con
WB and real-time PCR	6	6	6	6	6	6
FISH	6	6	6	6	6	6
FG + CTb	6	6				
BDA	6	6				

Abbreviations: BDA, animals were injected biotinylated dextran amine (BDA) into the dorsomedial part of the principal sensory trigeminal nucleus (Vpdm); Con, the age matched control group; FG + CTb, animals were injected cholera toxin B subunit (CTb) into the inferior alveolar nerve, and fluoro-gold (FG) into the cerebellum; FISH, fluorescence in situ hybridization; UAC, the unilateral anterior crossbite (UAC) group; WB, Western blot; real-time PCR, real-time polymerase chain reaction.

CTb into the inferior alveolar nerve and FG into the cerebellum; the other six rats in each of the UAC and control groups received injections of BDA into the Vpdm. These rats were sacrificed 1 week after the injections.

Details of the animal distribution in the main experimental groups and subgroups are presented in Table 1.

Unilateral anterior crossbite induction

A unilateral anterior crossbite was induced in experimental rats, as previously reported [36]. In brief, a section of metal tube with a length of 2.5 mm and an inside diameter of 3 mm was bonded onto the rat left maxillary incisor (Figure S1). A curved section of metal tube with a length of 4.5 mm and an inside diameter of 3.5 mm was adhered to the left mandibular incisor. The mandibular tube was bent to form a 135° curved and tilted occlusal plate (Figure S1). The tubes were carefully checked every other day. The UAC model was maintained during the entire experimental period. Control rats had no metal tubes adhered.

Cholera toxin B subunit/fluorogold (CTb/FG) and biotinylated dextran amine (BDA) injection

Rats were injected with CTb/FG and BDA one week after UAC induction. For CTb/FG injection, the rats were anaesthetized by intraperitoneal injection with sodium pentobarbital (35 mg/kg of body weight). Then, rats were placed on a stereotaxic frame (RWD Life Science). FG was injected stereotactically via a glass micropipette (tip-diameter 10–15 μm) (Hamilton Robotics) into the cerebellum at the following coordinates: 11.7 mm caudal to Bregma; 4.5 mm lateral to the midline; and 4.6 mm in depth from the brain surface based on the rat brain atlas. For CTb injection, as

previously reported [25], a small bone window was drilled into the oral and facial mandibular ramus to fully observe and expose the inferior alveolar nerve. The nerve was separated from the surrounding blood vessels. A glass micropipette with an internal tip diameter of 15–20 μm, attached to a 10 μl Hamilton micro syringe (Hamilton Robotics), filled with 6–8 μl of 1% CTb (Sigma) dissolved in distilled water was injected into the inferior alveolar nerve. The distal segment of the inferior alveolar nerve was ligated after the injection. The rats injected with CTb/FG were sampled 1 week later.

For a single injection of BDA in the Vpdm, the rats underwent the same procedure as were used under the FG method. The Vpdm was located at the level of the pons, from the rostral side of the Vme to the rostral subnucleus of the spinal trigeminal nucleus. The Vpdm injection site is at the following coordinates: 10.0 mm caudal to Bregma; 2.8 mm lateral to the midline; and 8.6 mm ventral to the brain surface based on the rat brain atlas. The rats were sampled 1 week later. Only data collected from rats in which the injection areas were the correct regions were used for further analysis.

Sampling

For histology, rats injected with CTb/FG or BDA were euthanized by intraperitoneal injection with an overdose of sodium pentobarbital (100 mg/kg of body weight). The blood was rinsed with 0.1 mol/L phosphate-buffered saline and then with a buffer containing 4% paraformaldehyde; 15% saturated picric acid was used in 500 ml phosphate buffer (pH 7.2–7.4) for fixation during perfusion. The brains were carefully removed and post-fixed in the same fixative for 2 h and then placed at 4°C overnight with 0.1 M phosphate buffer containing 30% (w/v) sucrose. The brain segments containing Vpdm and cerebellum were extracted and sliced into 25-μm-thick coronal sections with a Leica cryostat (Leica Biosystems). Vpdm tissue located between Bregma −9.36 mm and −10.32 mm was collected. Cerebellum tissue located between Bregma −9.6 mm and −13.68 mm was collected and divided into three subgroups: rostral (−9.6 mm to −10.96 mm), ventral (−10.96 mm to −12.32 mm), and caudal (−12.32 mm to −13.68 mm).

In situ hybridization immunofluorescence histochemistry

The hybridization procedure was based on the procedure described in a previous report [24]. A cDNA fragment of VGLUT1 (nucleotides 855–1788; GenBank accession number XM_133432.2) was cloned into the vector

pBluescriptII SK+ (Stratagene) as follows: sections of the Vpdm were hybridized with a VGLUT1 mRNA fluorescent tag RNA probe (including 0.5 g/ml) for 20 to 24 h in a mixed hybrid buffer at a temperature of 60°C. The hybridization buffer contained: 5×saline sodium citrate (sodium citrate buffer, 1×saline sodium citrate: 0.015 M sodium citrate and 0.15 M NaCl, pH = 7.0); 2% (w/v) blocking reagent (Roche Diagnostics); 50% (v/v) formamide; 0.1% (w/v) N-lauroylsarcosine; and 0.1% sodium dodecyl sulphate. After hybridization, the sections were washed with wash buffer 2×saline sodium citrate, 50% (v/v) formamide, and 0.1% N-lauroylsarcosine at 60°C for 20 min and then kept at 37°C with RNase A (10 µg/ml) in a mixture of 0.5 M sodium chloride, 0.01 M Tris–HCl (pH 8.0), and 1 mM ethylenediamine tetraacetic acid; finally, they were washed in 0.2×saline sodium citrate containing 0.1% (w/v) sodium N-lauroylsarcosine for 20 min. Subsequently, the sections were incubated overnight with 1:2000-diluted alkaline phosphatase conjugated anti-digoxigenin IgG Fab fragment (1093274; Roche Diagnostics) in 0.1 M Tris–HCl (pH 7.5)-buffered 0.9% (w/v) saline (pH 7.5) containing 1% blocking reagent. Then, the sections were washed with 0.15 M NaCl, 0.1 M Tris–HCl (pH 7.5), and 0.05% (v/v) Tween 20 and incubated for 3 h with fluorescein isothiocyanate-avidin conjugate (1:1000; Millipore). The sections were placed on gelatine-coated glass slides and observed under a confocal laser scanning microscope (FV1000; Olympus).

Light microscopy immunofluorescence histochemistry

For CTb- and FG-injected rats, sections containing Vpdm plane were selected for immunofluorescence staining of neuronal nuclei (NeuN)/CTb/FG and NeuN/CTb/VGLUT1, respectively. The experimental procedures were as follows: (i) rabbit anti-VGLUT1 IgG (1:500; Synaptic System)/rabbit anti-FG IgG, mouse anti-NeuN IgG (1:1000; Millipore), and goat anti-CTb IgG (1:2000; List Biological) were used to incubate slices at room temperature overnight, and (ii) Alexa488-conjugated donkey anti-goat IgG (1:500; Millipore), Cy3-conjugated donkey anti-rabbit IgG (1:1000; Millipore), and Alexa647-conjugated donkey anti-mouse IgG (1:500; Millipore) were used to incubate slices for 8 h. The diluent used in steps (i) and (ii) was 0.05 mol/L phosphate buffer saline (PBS) containing 5% donkey serum, 0.25% carrageenan, 0.05% sodium azide, and 0.5% Triton X-100.

Sections containing cerebellum of BDA-injected rats were processed for BDA, VGLUT1, and NeuN triple-immunofluorescence staining. The experimental procedures were as follows: incubation with mouse anti-NeuN IgG (1:1000; Millipore) and rabbit anti-VGLUT1 IgG (1:500;

Synaptic System) for 16–18 h at room temperature, followed by a mixture of fluorescein isothiocyanate-avidin conjugate (1:1000; Millipore), Cy3-conjugated donkey anti-rabbit IgG (1:1000; Millipore), and Alexa 647-conjugated donkey anti-mouse IgG (1:500; Millipore) for 4 h at room temperature. Immunohistochemical controls were performed by omission of the primary and the secondary antibody. The digital images were captured and processed using FV10-ASW 1.6 software (Olympus).

In the cell counting process, neuronal cell bodies were counted on 10 sections throughout the Vpdm and cerebellum in a series of 25-µm sections, which would cover the rostral-caudal axis of the Vpdm and cerebellum. The selection range of Vpdm tissue section count was 9.24 mm to 10.44 mm caudal to Bregma and the cerebellum ranged from 9.48 mm to 13.68 mm caudal to Bregma. Only immunopositive neurons in Vpdm and cerebellum with clear neuronal morphology were counted with the total number summarized. The number of neurons was counted on 10 sections from each rat, summed individually, and averaged per rat. The images obtained were used to document and analyse the ratio difference of triple-labelled neuron numbers in the UAC and control groups. Data were presented as the mean ± standard deviation (SD).

RNA extraction and real-time PCR assay

The brainstem was removed after perfusion with 200 ml of 5 mM PBS (pH 7.3). Tissue of Vpdm was collected from 10 cryosections located between Bregma −9.36 mm and −10.32 mm. The cerebellum was collected between Bregma −9.7 mm and −13 mm. RNA was isolated using TRIzol (Invitrogen) and purified with the RNeasy Mini Kit (Qiagen). The Applied Bio systems 7500 Real-time PCR machine (Applied Bio Systems) was used to analyse the gene expression. The primers for VGLUT1 target genes are GAGTCACCTGCACTACACCC (forward) and TGAGGAACACGTACTGCCAC (reverse; GenBank accession no. NM_053859.2).

Western blot analysis

According to the standard Western blot protocol, tissues at the level of the Vpdm and cerebellum from the brainstem were removed carefully. To obtain total protein extracts, samples were homogenized in extraction buffer, including 20 mM Tris–HCl (pH 7.4), 5 mM ethylenediamine tetraacetic acid, 140 mM NaCl, 1% Triton X-100, 1 mM sodium vanadate, 1 mM phenylmethylsulfonyl fluoride, 10 mM sodium fluoride, and 1 mg/ml aprotinin at 4°C. The samples were centrifuged at 12,000 g at 4°C for 20 min, and the

supernatant was carefully absorbed and placed in precooled centrifuge tubes. The supernatant was measured by the Bio-Rad Protein Assay kit (Bio-Rad) and denatured at 95°C for 5 min. After proteins were fractionated by sodium dodecyl sulfate-polyacrylamide gel electropheresis, they were transferred onto an Immobilon-P membrane. The membrane was sealed with skim milk for 2 h and incubated overnight at 4°C with primary antibodies. The protein from Vpdm/cerebellum was incubated with mouse anti-β-actin (1:2000; Santa Cruz Biotechnology) and mouse anti-VGLUT1 (1:500; Millipore). The blots were detected using a horseradish peroxidase-conjugated secondary antibody and chemiluminescence.

Statistical analysis

After a database of the results was set up, the SPSS 17.0 package (SPSS) was used to describe and analyse the data. Data acquisition and analysis were performed blindly, and data are presented as the mean ±standard deviation. Two-way analysis of variance (ANOVA) with Bonferroni's multiple comparison tests was used for between-group comparisons (for example, the analysis of Western blot and real-time PCR data with experimental group and time as the main effects). The statistical significance level was defined as $p < 0.05$.
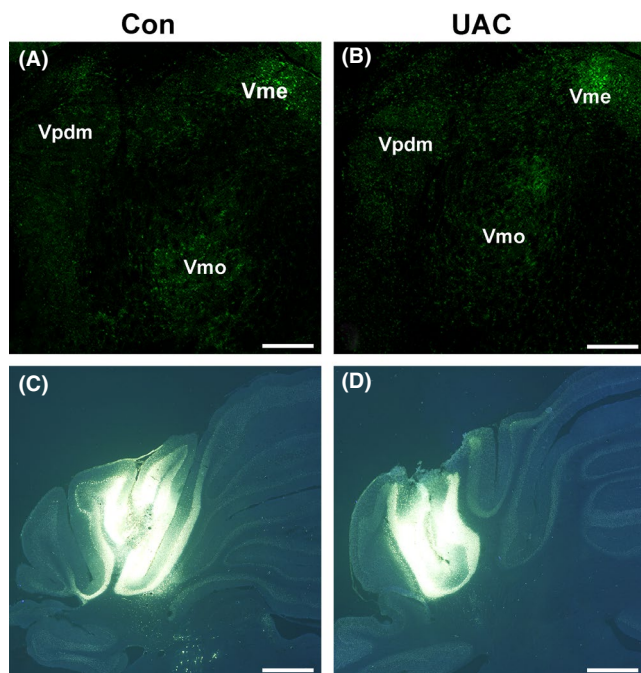
FIGURE 1 Fluorescent photomicrographs observation of the injection of cholera toxin B subunit (CTb) and fluoro-gold (FG). Representative trigeminal mesencephalic nucleus (Vme) profile after injection of CTb in the inferior alveolar nerve (A,B) and FG injection site of the lateral cerebellum (C,D). Vmo, the trigeminal motor nuclei. Scale bars = 200 μm

RESULTS

Effect of unilateral anterior crossbite on the Vpdm-cerebellum pathway

The rats in the UAC and control groups were successfully injected with CTb into the inferior alveolar nerve (Figure 1A,B) and with FG into the cerebellum (Figure 1C,D). Many axon terminals around the neurons in the Vpdm on the side ipsilateral to the injection were labelled anterogradely with CTb and retrogradely with FG (Figure 2A–D). In the UAC group, the average number of NeuN/CTb/FG triple-labelled neurons in Vpdm was 76.00 ± 4.00, accounting for 23.63 ± 0.90 (%) of the number of FG positive neurons; meanwhile, in the control group, they amounted to 39.00 ± 2.65 and 16.33 ± 0.69 (%), respectively (Figure 2E,F; $p < 0.01$).

Effect of unilateral anterior crossbite on VGLUT1 protein expression in the Vpdm

In the rats injected with CTb into the inferior alveolar nerve, some of the CTb-labelled axonal profiles in the Vpdm were VGLUT1 immunopositive. Many CTb and VGLUT1 double-labelled axonal profiles were in close proximity to NeuN-immunopositive neuronal profiles, as revealed by triple-immunofluorescence staining of CTb, VGLUT1, and NeuN (Figure 3A–D). In the UAC group, the average number of NeuN/CTb/VGLUT1 triple-labelled neurons in Vpdm was 175.00 ± 21.00, accounting for 29.10 ± 5.00 (%) of the number of CTb positive neurons; meanwhile, in the control group, they were 61.67 ± 11.10 and 16.30 ± 0.80 (%), respectively (Figure 3E,F; $p < 0.05$). The differences were confirmed by Western blot assays, which revealed that the protein expression level of VGLUT1 in the Vpdm was higher in the UAC group at all three time points (2, 4, and 8 weeks) (Figure 4A,B; $p < 0.01$).

Effect of unilateral anterior crossbite on Vpdm and VGLUT1 expression in the cerebellum
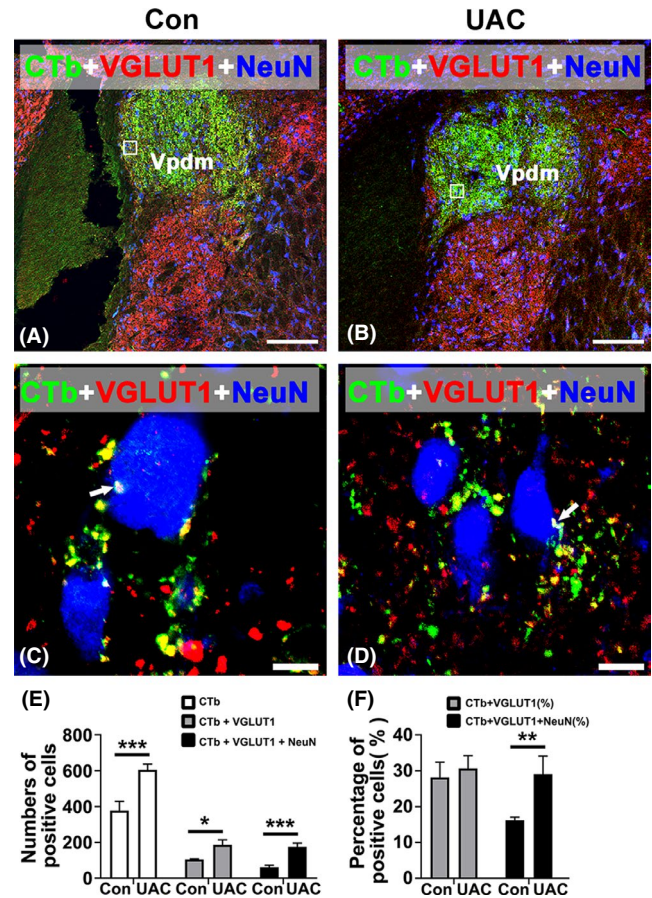
The mRNA expression of VGLUT1 in the Vpdm was examined by in situ hybridization histochemistry using digoxigenin (Figure 5A). Quantitative real-time PCR data indicated that the expression level of VGLUT1 mRNA in the UAC groups was markedly higher than that of the control groups at all three time points (2, 4, and 8 weeks) (Figure 5B; $p < 0.05$).

In BDA-injected rats, many axon terminals in the cerebellum on the side ipsilateral to the injection were labelled anterogradely with BDA (Figure 6A,B). Some of the BDA-labelled axonal profiles in the cerebellum were VGLUT1 immunopositive (Figure 6C,D). The BDA and VGLUT1 double-labelled axonal
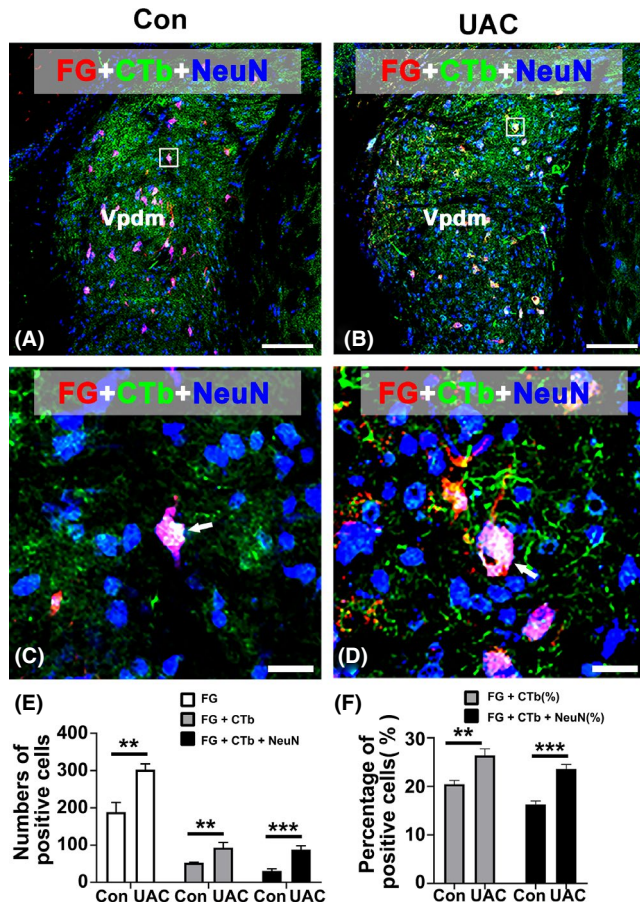
FIGURE 2 Triple-immunofluorescence histochemistry for the cholera toxin B subunit (CTb) (green), fluoro-gold (FG) (red), and neuronal nuclei (NeuN) (blue) in a transverse section through the dorsomedial part of the principal sensory trigeminal nucleus (Vpdm) from a rat in which CTb was injected into the inferior alveolar nerve and FG into cerebellum of unilateral anterior crossbite (UAC) and control (Con) groups. The framed areas in panels (A) and (B) are magnified in panels (C) and (D), respectively. White arrows indicate neurons dually labelled with FG (red) and NeuN (blue), which are merged (pink) and in close apposition to CTb-positive axonal profiles (green). (E) FG+CTb (%) indicate the percentage of FG/CTb double-labelled neurons to total number of FG-labelled neurons; (F) FG+CTb+NeuN (%) indicate the percentage of FG/CTb/NeuN triple-labelled neurons to total number of FG-labelled neurons. Scale bars: 200 µm in images (A) and (B) and 10 µm in images (C) and (D). $n = 6$/group. ** $p < 0.01$, *** $p < 0.001$
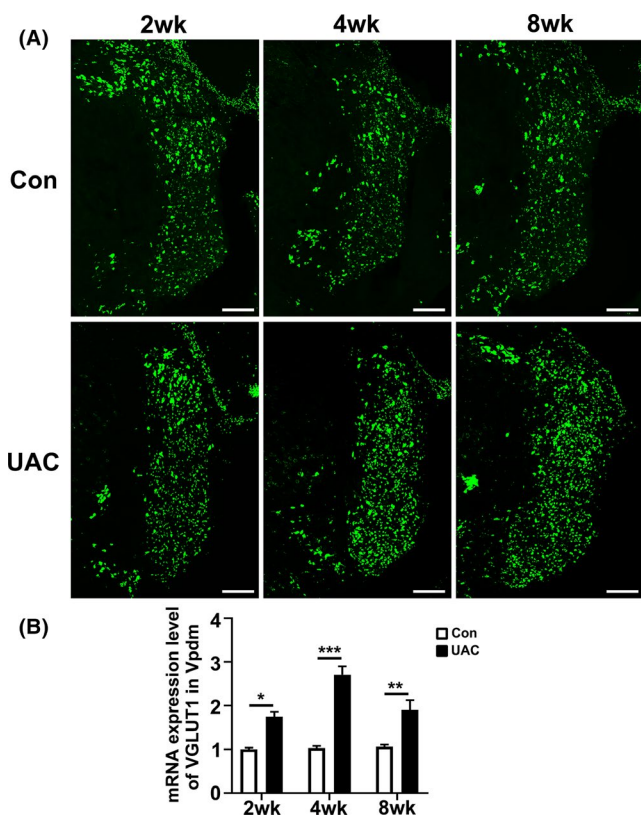

FIGURE 3 Comparison of vesicular glutamate transporter 1 (VGLUT1) expression in the dorsomedial part of the principal sensory trigeminal nucleus (Vpdm) between the unilateral anterior crossbite (UAC) and control (Con) groups. (A–D) Triple-immunofluorescence histochemistry for the cholera toxin B subunit (CTb) (green), vesicular glutamate transporter 1 (VGLUT1) (red), and neuronal nuclei (NeuN) (blue) in a transverse section through the trigeminal mesencephalic nucleus (Vme) and Vpdm from a rat in which CTb was injected into the inferior alveolar nerve. The framed areas in images (A) and (B) are magnified in images (C) and (D), respectively. White arrows indicate axonal profiles double-labelled with VGLUT1 and CTb, which are merged (yellow) and in close apposition to NeuN. (E) CTb+VGLUT1(%) indicate the percentage of CTb+VGLUT1 double-labelled neurons to total number of CTb-labelled neurons; (F) CTb+VGLUT1+NeuN (%) indicate the percentage of CTb/GLUT1/ NeuN triple-labelled neurons to total number of CTb-labelled neurons. Scale bars: 200 µm in images (A) and (B) and 10 µm in images (C) and (D). $n = 6$/group. * $p < 0.05$, ** $p < 0.01$, *** $p < 0.001$

profiles were in close apposition to NeuN-immunopositive neuronal profiles, as revealed by triple-immunofluorescence staining (Figure 6E,F). In the UAC group, the average number of NeuN/BDA/VGLUT1 triple-labelled neurons in the cerebellum was 232.33 ± 9.01, accounting for 21.23 ± 1.54 (%) of the number of BDA positive neurons; meanwhile, in the control group, they were 61.00 ± 5.57 and 8.38 ± 2.67 (%), respectively (Figure 6G,H; $p < 0.001$). Western blot data indicated

the increase of VGLUT1 protein expression in the cerebellum of UAC rats at 2, 4, and 8 weeks (Figure 7A,B; $p < 0.05$). Quantitative real-time PCR data indicated that the expression of VGLUT1 mRNA in the cerebellum of the UAC groups was markedly higher than that of the control groups at 2, 4, and 8 weeks (Figure 7C; $p < 0.01$).
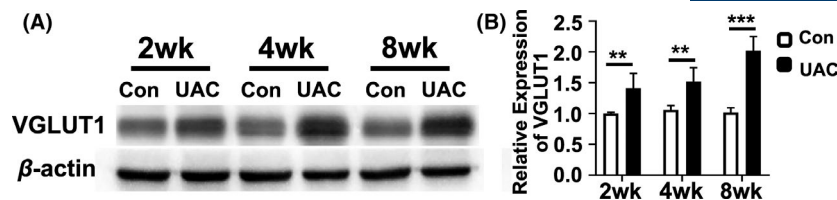
FIGURE 4 (A) The protein expression of vesicular glutamate transporter 1 (VGLUT1) in the dorsomedial part of the principal sensory trigeminal nucleus (Vpdm) as revealed by Western blot assay. (B) Data are presented as the mean ±standard deviation. $n = 6$/group. **$p < 0.01$, ***$p < 0.001$

FIGURE 5 Comparison of the mRNA expression level of vesicular glutamate transporter 1 (VGLUT1) expressed in the dorsomedial part of the principal sensory trigeminal nucleus (Vpdm) between the unilateral anterior crossbite (UAC) and control (Con) groups. (A) In situ hybridization immunofluorescence of histochemical sections showing the hybridization signals in the cell bodies of Vpdm neurons. Scale bar = 200 μm. (B) Real-time PCR of the levels of VGLUT1 expressed in Vpdm neurons. Data are presented as the mean ±standard error. $n = 6$/group. *$p < 0.05$, **$p < 0.01$, ***$p < 0.001$

DISCUSSION

Even though the electrophysiological/calcium imaging study is required to determine with certainty the impact of UAC on the Vpdm-cerebellum circuit, the present morphological data obtained from BDA, CTb, and FG tracing, together with the VGLUT1 expression at protein and mRNA levels, indicate the activation of the Vpdm-cerebellum pathway by UAC. The excitation impact of UAC on the Vpdm-cerebellum circuit is supported by the increased VGLUT1 protein and mRNA expression in the Vpdm and cerebellum. Our data provide evidence that changes in occlusion (such as UAC) alter the functional state of cerebellum, which might have an impact on body posture balance.

The cerebellum is involved in multiple phases of motor control, including planning, execution, and long-term error correction [37]. Literature regarding the relationship between the stomatognathic system and body posture has grown at a fast rate in recent years. Conflicting data has been also reported. Results of recent reviews have been diverse with respect to this clinical correlation [38]. The dental occlusion contribution to postural control has been proposed to depend on external disturbances [39,40]. Our published data [14,25,35,41] and the present work bring about supportive evidence. The existence of an ascending pathway mediating proprioception from the periodontal region to the cerebellum provides a possible neuroanatomical basis for the trigeminal mechanism of somatic movement and balance. These changes should be minor during the present experimental period because we did not notice any obvious mobility problems in the animals; however, osteoarthritis, like lesions [29,32], injury [26] and atrophy of masseters [27] was significant in UAC treated rats.

The pathways sending the excitatory message to Vpdm remain unidentified by the current data. It has been indicated that, in the proprioceptive pathway of the fifth nerve, there are direct projections from neurons of Vme to the Vpdm in the rats [13,42,43]. The primary neurons of the Vme form a mediolaterally narrow band of neurons located within all rostro-caudal levels of the entire midbrain [42]. This makes it possible for the projections of neurons in the Vme to target many other neurons in the brainstem. The neurons of Vme innervate spindles in the jaw-closing muscles and periodontal pressoreceptors [25,35,41,43]. Axons involved in trigeminal proprioception from periodontal mechanoreceptors and spindles in the jaw-closing muscles directly bypass the trigeminal ganglion and leave their cell bodies in all the rostro-caudal levels of the entire mesencephalon [44]. Hence, Vpdm in UAC rats could be excited via the Vme pathway.
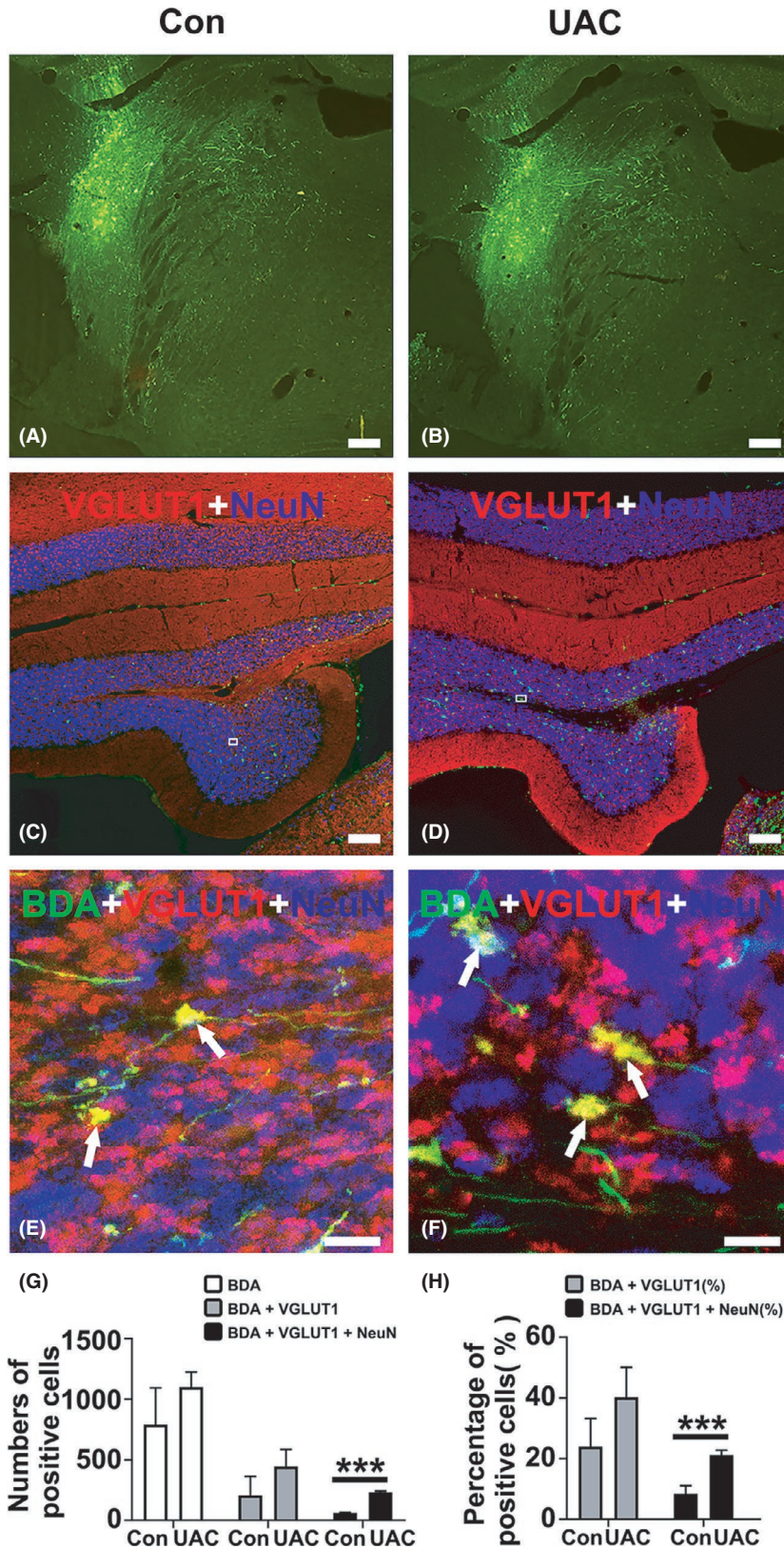
FIGURE 6 Projection fibres from the dorsomedial part of the principal sensory trigeminal nucleus (Vpdm) to the cerebellum and excitation stimulated by unilateral anterior crossbite (UAC). Anterograde tracing of projection fibres from the Vpdm to the cerebellum with biotinylated dextran amine (BDA) in the control (Con) group (A) and UAC group (B). BDA-positive terminals are observable in the cerebellum (C,D). The immunoreactivities for vesicular glutamate transporter 1 (VGLUT1) (red), BDA (green), and neuronal nuclei (NeuN) (blue) positive in the cerebellum are presented. White arrows indicate axonal profiles triple-labelled with VGLUT1 (red) and BDA (green), which are merged (yellow) and in close apposition to NeuN (blue). The framed areas in panels (C) and (D) are magnified in (E) and (F). (G) BDA+VGLUT1 (%) indicate the percentage of BDA+VGLUT1 double-labelled neurons to total number of BDA-labelled neurons; (H) BDA+VGLUT1+NeuN (%) indicate the percentage of BDA/VGLUT1/NeuN triple-labelled neurons to total number of BDA-labelled neurons. Scale bars: 200 μm in images (A–D) and 10 μm in images (E) and (F). $n = 6$/group. ***$p < 0.001$

There are several limitations and implications of the present work. Firstly, female animals were used, as it has been done in our serial studies on the UAC model [26–32]. We used female animals to reduce the impact of the complex sex factors. Secondly, the neurons in the Vme are not only stimulated by the peripheral afferents from proprioception receptors of periodontal ligament, but also by the afferents from the spindles in jaw muscles [44]. Thirdly, the primary afferent neurons of the trigeminal nerve (a group of neural crest-derived sensory neurons) are located in the Vme and

FIGURE 7 Comparison of the protein and mRNA expression levels of vesicular glutamate transporter 1 (VGLUT1) in the cerebellum between the unilateral anterior crossbite (UAC) and control (Con) groups at 2, 4, and 8 weeks, as revealed by Western blot (A, B) and real-time PCR (C). Data are presented as the mean ±standard deviation. $n = 6$/group. *$p < 0.05$, **$p < 0.01$, ***$p < 0.001$
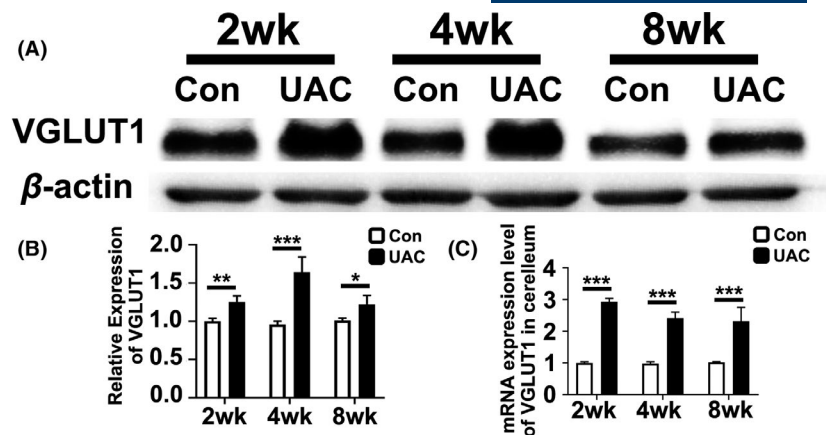
in the trigeminal ganglion. The primary afferents from the trigeminal ganglions carry somatosensory information from mechanoreceptors, thermoreceptors, and nociceptors in the face, oral, and nasal cavities [44], while afferents from neurons in Vme convey the proprioception. By injection of CTb into the inferior alveolar nerve (as done in the present study), neurons of the trigeminal ganglions could also be insulted. Hence, presently, both Vme and trigeminal ganglions are able to send excitatory messages to Vpdm in UAC rats. However, the involvement of the trigeminal ganglion in the present UAC model remains an open question.

Overall, these data help to understand a possible neurobiological mechanism involving persistent stimulation by the occlusion, which ultimately has an impact on the neuronal excitation of the cerebellum through the Vpdm-cerebellum circuit and may be a factor in eliciting related symptoms, such as body posture imbalance.

ACKNOWLEDGEMENTS

CONFLICT OF INTERESTS

The authors declare no potential conflicts of interest with respect to the authorship and/or publication of this article.

AUTHOR CONTRIBUTIONS

MS: Conceptualization, Methodology, Data curation, Investigation, Formal analysis, Writing – original draft, Visualization; **XL**: Conceptualization, Methodology, Data curation, Investigation, Formal analysis, Writing – original draft, Visualization; **JL**: Conceptualization, Methodology, Writing – original draft, Project administration, Resources; **MW**: Conceptualization, Methodology, Writing – original draft, Funding acquisition, Project administration, Resources, Supervision, Visualization; **CZ**: Data curation, Investigation, Formal analysis, Writing – review and editing, Software; **HZ**: Data curation, Investigation, Formal analysis, Writing – review and editing, Validation; **QL**: Formal analysis, Writing – review and editing, Validation; **DW**: Formal analysis, Writing – review and editing; **XiaL**: Formal analysis, Writing – review and editing.

ORCID

Minghong Shi https://orcid.org/0000-0002-7689-435X
Xin Liu https://orcid.org/0000-0001-8655-5645
Chunkui Zhang https://orcid.org/0000-0003-0492-3876
Hongyun Zhang https://orcid.org/0000-0002-8955-1460
Qian Liu https://orcid.org/0000-0002-7858-7089
Dongmei Wang https://orcid.org/0000-0002-3292-8474
Xiaodong Liu https://orcid.org/0000-0002-3434-1706
Jinlian Li https://orcid.org/0000-0003-4304-8058
Meiqing Wang https://orcid.org/0000-0002-7373-385X

REFERENCES

1. Lund JP. Mastication and its control by the brain stem. Crit Rev Oral Biol Med. 1991;2:33–64.
2. Lazarov N. Fine structure and synaptic organization of the mesencephalic trigeminal nucleus of the cat: a quantitative electron microscopic study. Eur J Morphol. 1996;34:95–106.
3. Gadotti ICBF, Biasotto-Gonzalez D. Preliminary rapport on head posture and muscle activity in subjects with class I and II. J. Oral Rehabil. 2005;32:794–9.
4. D'Attilio M, Caputi S, Epifania E, Festa F, Tecco S. Evaluation of cervical posture of children in skeletal class I, II, and III. Cranio. 2005;23:219–28.
5. Festa F, Tecco S, Dolci M, Ciufolo F, Di Meo S, Filippi MR, et al. Relationship between cervical lordosis and facial morphology in Caucasian women with a skeletal class II malocclusion: a cross-sectional study. Cranio. 2003;21:121–9.
6. Julià-Sánchez S, Álvarez-Herms J, Cirer-Sastre R, Corbi F, Burtscher M. The influence of dental occlusion on dynamic balance and muscular tone. Front Physiol. 2019;10:1626.
7. Grosdent S, O'Thanh R, Domken O, Lamy M, Croisier JL. Dental occlusion influences knee muscular performances in asymptomatic females. J Strength Cond Res. 2014;28:492–8.

8. Michelotti A, Rongo R, D'Antò V, Bucci R. Occlusion, orthodontics, and temporomandibular disorders: cutting edge of the current evidence. J World Fed Orthod. 2020;9:S15–8.

9. Marchena-Rodriguez A, Moreno-Morales N, Ramirez-Parga E, Labajo-Manzanares MT, Luque-Suarez A, Gijon-Nogueron G. Relationship between foot posture and dental malocclusions in children aged 6 to 9 years: a cross-sectional study. Medicine. 2018;97:e0701.

10. Leroux E, Leroux S, Maton F, Ravalec X, Sorel O. Influence of dental occlusion on the athletic performance of young elite rowers: a pilot study. Clinics. 2018;73:e453.

11. Hirase T, Inokuchi S, Matsusaka N, Nakahara K, Okita M. Effects of a resistance training program performed with an interocclusal splint for community-dwelling older adults: a randomized controlled trial. J Phys Ther Sci. 2016;28:1499–504.

12. Baumann O, Borra RJ, Bower JM, Cullen KE, Habas C, Ivry RB, et al. Consensus paper: the role of the cerebellum in perceptual processes. Cerebellum. 2015;14:197–220.

13. Luo PF, Wang BR, Peng ZZ, Li JS. Morphological characteristics and terminating patterns of masseteric neurons of the mesencephalic trigeminal nucleus in the rat: an intracellular horseradish peroxidase labeling study. J Comp Neurol. 1991;303:286–99.

14. Ge SN, Li ZH, Tang J, Ma Y, Hioki H, Zhang T, et al. Differential expression of VGLUT1 or VGLUT2 in the trigeminothalamic or trigeminocerebellar projection neurons in the rat. Brain Struct Funct. 2014;219:211–29.

15. Darian-Smith I, Phillips G. Secondary neurones within a trigeminocerebellar projection to the anterior lobe of the cerebellum in the cat. J Physiol. 1964;170:53–68.

16. Van Ham JJ, Yeo CH. Somatosensory trigeminal projections to the inferior olive, cerebellum and other precerebellar nuclei in rabbits. Eur J Neurosci. 1992;4:302–17.

17. Bai L, Xu H, Collins JF, Ghishan FK. Molecular and functional analysis of a novel neuronal vesicular glutamate transporter. J Biol Chem. 2001;276:36764–9.

18. Wojcik SM, Rhee JS, Herzog E, Sigler A, Jahn R, Takamori S, et al. An essential role for vesicular glutamate transporter 1 (VGLUT1) in postnatal development and control of quantal size. Proc Natl Acad Sci USA. 2004;101:7158–63.

19. Liguz-Lecznar M, Skangiel-Kramska J. Vesicular glutamate transporters (VGLUTs): the three musketeers of glutamatergic system. Acta Neurobiol Exp (Wars). 2007;67:207–18.

20. Fremeau RT Jr, Voglmaier S, Seal RP, Edwards RH. VGLUTs define subsets of excitatory neurons and suggest novel roles for glutamate. Trends Neurosci. 2004;27:98–103.

21. Pang YW, Li JL, Nakamura K, Wu S, Kaneko T, Mizuno N. Expression of vesicular glutamate transporter 1 immunoreactivity in peripheral and central endings of trigeminal mesencephalic nucleus neurons in the rat. J Comp Neurol. 2006;498:129–41.

22. Kaneko T, Itoh K, Shigemoto R, Mizuno N. Glutaminase-like immunoreactivity in the lower brainstem and cerebellum of the adult rat. Neuroscience. 1989;32:79–98.

23. Magnusson KR, Clements JR, Larson AA, Madl JE, Beitz AJ. Localization of glutamate in trigeminothalamic projection neurons: a combined retrograde transport-immunohistochemical study. Somatosens Res. 1987;4:177–90.

24. Ge SN, Ma YF, Hioki H, Wei YY, Kaneko T, Mizuno N, et al. Coexpression of VGLUT1 and VGLUT2 in trigeminothalamic projection neurons in the principal sensory trigeminal nucleus of the rat. J Comp Neurol. 2010;518:3149–68.

25. Liu X, Zhang C, Wang D, Zhang H, Liu X, Li J, et al. Proprioceptive mechanisms in occlusion-stimulated masseter hypercontraction. Eur J Oral Sci. 2017;125:127–34.

26. Zhang HY, Yang HX, Liu Q, Xie MJ, Zhang J, Liu X, et al. Injury responses of Sprague-Dawley rat jaw muscles to an experimental unilateral anterior crossbite prosthesis. Arch Oral Biol. 2020;109:104588.

27. Zhang HY, Duan J, Wang J, Xie MJ, Liu Q, Liu JQ, et al. Masseter response to long-term experimentally induced anterior crossbite in Sprague-Dawley rats. Arch Oral Biol. 2020;122:104985.

28. Yang H, Wen Y, Zhang M, Liu Q, Zhang H, Zhang J, et al. MTORC1 coordinates the autophagy and apoptosis signaling in articular chondrocytes in osteoarthritic temporomandibular joint. Autophagy. 2020;16:271–88.

29. Zhang J, Liao L, Zhu J, Wan X, Xie M, Zhang H, et al. Osteochondral interface stiffening in mandibular condylar osteoarthritis. J Dent Res. 2018;97:563–70.

30. Zhang M, Yang H, Wan X, Lu L, Zhang J, Zhang H, et al. Prevention of injury-induced osteoarthritis in rodent temporomandibular joint by targeting chondrocyte CaSR. J Bone Miner Res. 2019;34:726–38.

31. Zhang M, Yang H, Lu L, Wan X, Zhang J, Zhang H, et al. Matrix replenishing by BMSCs is beneficial for osteoarthritic temporomandibular joint cartilage. Osteoarthritis Cartilage. 2017;25:1551–62.

32. Zhang M, Wang H, Zhang J, Zhang H, Yang H, Wan X, et al. Unilateral anterior crossbite induces aberrant mineral deposition in degenerative temporomandibular cartilage in rats. Osteoarthritis Cartilage. 2016;24:921–31.

33. Zhang J, Luo P, Pendlebury WW. Light and electron microscopic observations of a direct projection from mesencephalic trigeminal nucleus neurons to hypoglossal motoneurons in the rat. Brain Res. 2001;917:67–80.

34. Zhang J, Yang R, Pendlebery W, Luo P. Monosynaptic circuitry of trigeminal proprioceptive afferents coordinating jaw movement with visceral and laryngeal activities in rats. Neuroscience. 2005;135:497–505.

35. Liu X, Zhang C, Liu Q, Zhou K, Yin N, Zhang H, et al. Dental malocclusion stimulates neuromuscular circuits associated with temporomandibular disorders. Eur J Oral Sci. 2018;126:466–75.

36. Zhang X, Dai J, Lu L, Zhang J, Zhang M, Wang Y, et al. Experimentally created unilateral anterior crossbite induces a degenerative ossification phenotype in mandibular condyle of growing Sprague-Dawley rats. J Oral Rehabil. 2013;40:500–8.

37. Maurer C, Heller S, Sure JJ, Fuchs D, Mickel C, Wanke EM, et al. Strength improvements through occlusal splints? The effects of different lower jaw positions on maximal isometric force production and performance in different jumping types. PLoS One. 2018;13:e0193540.

38. Manfredini D, Castroflorio T, Perinetti G, Guarda-Nardini L. Dental occlusion, body posture and temporomandibular disorders: where we are now and where we are heading for. J Oral Rehabil. 2012;39:463–71.

39. Michelotti A, Buonocore G, Manzo P, Pellegrino G, Farella M. Dental occlusion and posture: an overview. Prog Orthod. 2011;12:53–8.

40. Julià-Sánchez S, Álvarez-Herms J, Burtscher M. Dental occlusion and body balance: a question of environmental constraints? J Oral Rehabil. 2019;46:388–97.

41. Liu X, Zhou KX, Yin NN, Zhang CK, Shi MH, Zhang HY, et al. Malocclusion generates anxiety-like behavior through a putative lateral habenula-mesencephalic trigeminal nucleus pathway. Front Mol Neurosci. 2019;12:174.

42. Luo P, Dessem D. Inputs from identified jaw-muscle spindle afferents to trigeminothalamic neurons in the rat: a double-labeling study using retrograde HRP and intracellular biotinamide. J Comp Neurol. 1995;353:50–66.

43. Luo P, Dessem D. Morphological evidence for recurrent jaw-muscle spindle afferent feedback within the mesencephalic trigeminal nucleus. Brain Res. 1996;710:260–4.

44. Lazarov NE. Neurobiology of orofacial proprioception. Brain Res Rev. 2007;56:362–83.

SUPPORTING INFORMATION

Additional supporting information may be found online in the Supporting Information section.